Numerical integration of high-order variational equations of ODEs

Article *in* Applied Mathematics and Computation · April 2023

DOI: 10.1016/j.amc.2022.127743

5 authors, including:

Angel Jorba
University of Barcelona
168 PUBLICATIONS **3,857** CITATIONS
SEE PROFILE

Marc Jorba
CRM Centre for Mathematical Research
23 PUBLICATIONS **98** CITATIONS
SEE PROFILE

Numerical integration of high-order variational equations of ODEs

Joan Gimeno[(1)] Àngel Jorba[(1)] Marc Jorba-Cuscó[(2)] Narcís Miguel[(3)]
Maorong Zou[(4)]

September 26, 2022

(1) Departament de Matemàtiques i Informàtica, Universitat de Barcelona, Gran Via de les Corts Catalanes, 585, 08007 Barcelona, Spain, {joan,angel}@maia.ub.es
(2) Centre de Recerca Matemàtica (CRM),
Edifici C, Campus UAB, 0 Floor, 08193 Bellaterra, Barcelona, Spain mjorba@crm.cat
(3) PAL Robotics S.L., Carrer de Pujades, 77, 4-4, 08005 Barcelona, Spain
narcis.miguel@pal-robotics.com
(4) Department of Mathematics, University of Texas at Austin, Austin, TX 78712, USA,
mzou@math.utexas.edu

Abstract

This paper discusses the numerical integration of high-order variational equations of ODEs. It is proved that, given a numerical method (say, any Runge-Kutta or Taylor method), to use automatic differentiation on this method (that is, using jet transport up to order p with a time step h for the numerical integration) produces exactly the same results as integrating the variational equations up to of order p with the same method and time step h as before. This allows to design step-size control strategies based on error estimates of the orbit and of the jets. Finally, the paper discusses how to use jet transport to obtain power expansions of Poincaré maps (either with spatial or temporal Poincaré sections) and invariant manifolds. Some examples are provided.

Keywords: Jet transport | Variational equations | Poincaré map | Parametrization method.

1 Introduction

It is well-known that invariant objects (equilibrium points, periodic orbits, invariant tori and their stable/unstable manifolds) play a key role in the understanding of the global properties of a dynamical system. They can be seen as the skeleton of the dynamics and, therefore, their knowledge provides insight on the properties of the system. To have a complete and reliable picture of the dynamics, it is common to combine theoretical results with numerical methods to analyze these manifolds.

To study dynamical systems defined as the flow of an Ordinary Differential Equation (ODE) it is common to use suitable Poincaré sections. They reduce the dimensions (phase space and invariant objects) by one and usually simplify the use of numerical methods. One of the difficulties of using Poincaré maps is that it has to be computed by means of a numerical integration of the flow. When the derivatives of the Poincaré map are needed it is usual to resort to variational equations, whose numerical integration provides the derivatives of the flow with respect to initial

conditions and/or parameters: let us denote by $\Phi(t; t_0, x_0)$ the flow of the Initial Value Problem (IVP)

$$\dot{x} = f(t, x), \qquad x(t_0) = x_0. \tag{1}$$

Then, if we denote the matrix $D_{x_0}\Phi(t; t_0, x_0)$ as $V(t)$, it follows that V satisfies the linear differential equation $\dot{V} = D_x f(t, x(t))V$, where $x(t)$ is the solution of (1). These equations are usually written together in the form

$$\begin{aligned} \dot{x} &= f(t, x), & x(t_0) &= x_0, \\ \dot{V} &= D_x f(t, x)V, & V(t_0) &= I, \end{aligned}$$

where I denotes the identity matrix. Similarly, one can look at the differential equations satisfied by higher order derivatives of the flow Φ. However, they are usually complicated expressions involving high order derivatives of f.

There are several situations in which high order derivatives of a Poincaré map are needed. One of them is the computation of high order approximation to invariant manifolds by means of the parametrization method [HCL$^+$16]. The main idea of the parametrization method is to look for a suitable parametrization of the required manifold. For instance, under generic conditions, the stable and unstable manifolds of a fixed point can be represented as a high-order Taylor expansion w.r.t. a parameter along the manifold. Then, it can be seen that the coefficients of this Taylor expansion satisfy a set of linear equations. These equations involve high order derivatives of the map.

This paper focuses on the effective computation of high-order derivatives of stroboscopic and spatial Poincaré maps. We discuss, as a particular example, the computation of high-order approximations of stable/unstable manifolds of fixed points, which correspond to periodic orbits of the ODE flow. We are also interested on the efficiency, to allow the use of extended precision arithmetic when required. A similar process has already been applied for invariant manifolds of tori of stroboscopic maps [GJNO22]. The computation of invariant manifolds is a classical topic in dynamical systems, and the standard methods to compute them are based on computing first a linear approximation to the manifold and then to globalize it [Sim90, KOD$^+$05]. What we propose here is to compute first a high order approximation of the manifold and then to globalize it. The advantage of using a high order approximation is that we can start the globalization further away from the fixed point, and this: i) reduces the total computation time; and ii) increases the accuracy of the computed manifold. This is shown in Section 6.2 with the help on an example.

One of the main tools used here is automatic differentiation (AD) [Gri00], which is an alternative way of computing derivatives at a given point. It is based on replacing the arithmetic of real numbers of a given algorithm by a (truncated) formal power series arithmetic so that the same algorithm will produce not only the result of the algorithm but also its derivatives.

In this paper we use these ideas to compute the derivatives of a Poincaré map. As the numerical integration of the flow is written as a sequence of formulas, we can replace the floating point arithmetic by a truncated power series arithmetic with floating point coefficients. We prove that regardless of the numerical integrator –e.g. Runge-Kutta, Taylor, etc– the process can be implemented. Note that these ideas can be viewed as an extension of the phase space to propagate the derivatives of the flow in addition to the trajectory. We are going to refer to this technique as "jet transport" ([AFJ$^+$08, JPN10]) since the set of derivatives of a function on a point is sometimes called the jet of derivatives of the function at this point.

A natural question is the accuracy of the derivatives of the flow obtained by using automatic differentiation on a time stepper for ODEs. As usual, by accuracy we mean the difference between these values and the exact solution of the variational flow. The error introduced by the time stepper on the orbit is a well studied topic and its knowledge is used, for instance, to derive algorithms of step size control according to a prescribed threshold. If, for instance, the time stepper (with step h) has an error $O(h^p)$, do the derivatives of the flow w.r.t. initial conditions obtained by jet transport also have an error $O(h^p)$? Does this error depend on the order of the derivative? How to derive a suitable step size control for a time stepper that includes jet transport? These questions are also addressed in this paper. The answer comes from the fact (proved in Section 3) that the error in the derivatives obtained using jet transport is exactly the same as the error obtained when applying the time stepper (without jet transport) to the corresponding variational equations. Therefore, we can estimate the error in the coefficients of the jet using the same error formulas used to estimate the error of the orbit, since the coefficients of the jet coincide (exactly) with the values obtained applying the time stepper to the variational equations. In particular, if the error of the time stepper on the orbit is $O(h^p)$, the error on the derivatives of the flow obtained using jet transport is also $O(h^p)$. This implies that we can use the existing step size control strategies for general ODEs when using jet transport, handling the coefficients of the jets as the components of the solution of the variational equations.

There is a vast literature on the applications of the numerical integration of high-order variational equations. This contribution is also devoted to its combination with the parametrization method for the computation of the high-order approximation of invariant manifolds. It is worth noting that these techniques have been used to tackle problems that range from those that arise from the theory of dynamical systems to applications to astrodynamics and orbital mechanics. The following gives an overview to the reader of the state of the art of the topic.

Jet transport techniques can be used to study problems in computational dynamical systems. This allows to deal with high-order derivatives of solutions of ODE that can be used, e.g., in the following contexts:

- The non-integrability of Hamiltonian systems can be established by studying its high-order variational equations via the so-called Morales-Ramis and Morales-Ramis-Simó theories. See [MS09] and references therein, where these are applied and exemplified.

- Jet transport has been extensively used to cope with the problem of propagation of uncertainties, namely in the loss of accuracy for long term integrations due to the change of shape of the propagated set of initial conditions, [AFJ$^+$08, AFJ$^+$09, JPN10, ADLBZB10]. Jet transport allows to propagate not only an initial condition but a region whose shape is determined by some polynomial, see [PPMG13, PPGM18, VADLL13]. In [WDLA$^+$15], the authors present an automatic method of to split the propagated domains to increase accuracy. The method relies on detecting when the flow expansion with respect to initial conditions is no longer accurate enough, and to split the region into two subregions. Each subregion is further propagated using the same polynomial representation before the splitting, but centered on different point (on each subregion).

- These same ideas can be used to refine techniques for detecting invariant structures. These techniques, that include e.g. Fast Lyapunov Indicators (FLI for short), usually rely on linear approximations of the dynamics. By means of jet transport one can use high-order approximations to get a better insight of the dynamics, see [PPMG14, PPMG15].

From the perspective of applications to orbital mechanics problems, jet transport techniques are a tool that allows to refine and extend the results using reference solutions.

- The computation of collision probability can also be addressed using jet transport techniques, see, for instance, [MADLBZ15]. In this work, the authors look first for close approaches (regular integrations with standard double arithmetic), and then once closest approaches are detected, collision probabilities are computed via propagation of uncertainties using jet transport.

- Affine optimal control problems, that is, problems that can be set as the equations of motion being affine in the controls, have been dealt with and jet transport as well. Integration of high-order variational equations can be used to find expansions of the solutions of the optimal control problem around a reference trajectory. Examples of such systems are low thrust transfers, see [LABZB14].

- High-order numerical and analytical extended Kalman Filters are implemented using jet transport techniques to easily go to high-orders in the derivatives, to reduce computational effort and to improve accuracy. This is applied to orbit determination problems, see [VADLL14].

- Two-point boundary value problems are dealt with jet transport techniques. A reference solution is found via classical iterative methods. An expansion around this reference solution is computed transporting the Jet to high-orders to find close new solutions, obtained via evaluation of the obtained Taylor expansions, see [LAL08].

- Validation of a-posteriori theorems. In [CCGd22] the computation of high-order derivatives of a stroboscopic Poincaré map with extended arithmetic precision was used to validate the existence a KAM torus close to its breakdown in a quasi-conformally symplectic system. The norm computation of these derivatives were needed to verify the inequalities of an a-posteriori theorem in [CCd13].

- Jet transport has been used in computer assisted proofs, such as [KS17] and implemented in computational libraries and packages, such as [CAP].

This paper starts in Section 2 fixing the notation of basic notions in automatic differentiation. After that, Section 3 presents the main contribution of the paper showing that the use of jet transport is equivalent to integrate high-order variational flows. Section 4 applies the previous results to the computation of high-order derivatives of Poincaré maps which is later applied in Section 5 to the parametrization method. Finally, Section 6 shows some illustrative examples using all this new methodology.

2 Automatic differentiation and jet transport

Automatic differentiation is a technique used to obtain high-order derivatives of the output of a given algorithm with respect to the input, see [GC91, Gri00, Nau12]. In this section, we summarize the main ideas involved in this tool. An essential ingredient for the successful implementation of automatic differentiation is the manipulation of (formal) power series.

2.1 Formal power series in one variable

A formal power series in one variable s is an expression of the form

$$\sum_{k\geq 0} a_k s^k, \tag{2}$$

where the coefficients a_k belong to a field. If f is a C^∞ function defined on a neighborhood of 0, we can choose as a_k its k-th *normalized derivative*,

$$a_k = \frac{1}{k!} f^{(k)}(0),$$

and then (2) can be seen as a formal series that encodes the *jet* of derivatives of f at 0. The manipulation of formal power series goes back to L. Euler. A modern reference for the topic is, for instance, the book by D. Knuth [Knu98]. To discuss the arithmetic of formal power series, let us define

$$A = \sum_{k\geq 0} a_k s^k, \qquad B = \sum_{k\geq 0} b_k s^k, \qquad C = \sum_{k\geq 0} c_k s^k.$$

The basic operations of power series, $A \pm B$ and AB are defined in a natural way. If $b_0 \neq 0$, the quotient $C = A/B$ is obtained by writing $BC = A$ and taking the coefficients of degree k at both sides,

$$b_0 c_k + b_1 c_{k-1} + \cdots + b_k c_0 = a_k,$$

which implies

$$c_k = \frac{1}{b_0}(a_k - b_1 c_{k-1} - \cdots - b_k c_0),$$

and this allows to compute the coefficients c_k recursively, starting from $c_0 = a_0/b_0$.

Let us see how to perform other operations. For instance, let us focus on $C = A^\alpha$ for $\alpha \in \mathbb{R}$. We assume $\alpha \neq 0, 1$ (these two cases are trivial) and $a_0 \neq 0$. Taking formal derivatives w.r.t. s we obtain $C' = \alpha A^{\alpha-1} A'$ which implies $C'A = \alpha C A'$. Now we equate the coefficients of degree $k-1$ at both sides to obtain

$$\sum_{j=0}^{k} j c_j a_{k-j} = \alpha \sum_{j=0}^{k} (k-j) a_{k-j} c_j,$$

and, therefore

$$c_k = \frac{1}{k a_0} \sum_{j=0}^{k-1} [\alpha k - (\alpha+1)j] a_{k-j} c_j,$$

which allows to compute the coefficients c_k ($k \geq 1$) recursively starting from $c_0 = a_0^\alpha$. We note that this formula includes the inversion ($\alpha = -1$) and the square root ($\alpha = \frac{1}{2}$).

The same idea can be used to compute $C = h(A)$ when h is any function that satisfies a simple differential equation. This includes log, exp and the trigonometric functions.

Remark 1. As a formal series A codifies the derivatives of a C^∞ function f at, say, 0. The formal series $h(A)$ codifies the derivatives of the composition $h \circ f$ at 0. In other words, the operations with formal series can be seen as the "transport" of derivatives through these operations.

2.2 Formal power series in several variables

In a similar way, we can consider power series of n variables,

$$A = \sum_{m \geq 0} \sum_{|k|=m} a_k s^k, \tag{3}$$

where $k \in \mathbb{N}^n$, $|k| = k_1 + \cdots + k_n$ and $s^k = s_1^{k_1} \cdots s_n^{k_n}$. As before, if f is a C^∞ multivariate function defined on a neighborhood of 0, we can take

$$a_k = \frac{\partial^k f}{k_1! \cdots k_n!}(0),$$

then (3) encodes the jet of partial derivatives of f at 0. The arithmetic of multivariate power series is very similar to the case of one variable. As an example, let us show how to compute $C = A^\alpha$ for $\alpha \in \mathbb{R}$. As before, we assume $\alpha \neq 0, 1$. We replace s_j by $s_j z$ (z is an extra one-dimensional variable that, at the end, it will be selected equal to 1 to recover the initial form) and we obtain,

$$A = \sum_{m \geq 0} A_m z^m, \quad \text{where} \quad A_m = \sum_{|k|=m} a_k s^k.$$

Using the same notation for C, we can use the procedure derived in Section 2.1 to obtain,

$$C_m = \frac{1}{mA_0} \sum_{j=0}^{m-1} [\alpha m - (\alpha + 1)j] A_{m-j} C_j,$$

where now A_j and C_j denote homogeneous polynomials of degree j. As the only required operations are sums and products of homogeneous polynomials (note that A_0 appears in a denominator but it is always a number), the formula can be carried out easily. In the same way, similar formulas can be obtained for other operations. As in the one dimensional case, operations with multivariate formal series can be seen as the "transport" of partial derivatives through these operations.

2.3 Truncated power series

The computer implementation of these techniques is done using truncated power series. For instance, assume we are working with truncated series up to order, say, M. Then, the equality $C = A^\alpha$ means that C is a truncated power series whose coefficients coincide with the ones of A^α. Note that this does not mean that they coincide as functions of their variables (in fact they do not, since A^α contains terms of order higher than M that we are neglecting). We expect that this notation will not confuse the reader.

Note that the efficiency of the operations depends on the efficiency of the product of homogeneous polynomials. Moreover, note that the complexity of these operations is very low: for instance, the cost of A^α is similar to the cost of a product of two truncaded power series of order M. It is not difficult to see that this is the complexity of all the standard operations.

2.4 Jet transport

The automatic differentiation can be used on an algorithm for the numerical integrations of ODEs to compute the derivative of the final point of the orbit with respect to the the initial

data and/or parameters. More concretely, given an ODE, an initial condition (t_0, x_0) and a numerical method for ODEs, let us denote by $\Phi(t_0, x_0; h)$ the algorithm of numerical integration that, from the initial data (t_0, x_0) approximates the point of the orbit at time t_0+h. Jet transport is the result of using automatic differentiation on this algorithm, that is, to replace the usual floating point arithmetic by an arithmetic of power series, truncated at degree m. Then, running this algorithm on the data $(t_0, x_0 + s)$, where we assume $x_0 \in \mathbb{R}^n$ and $s = (s_1, \ldots, s_n)$ we obtain something like $x_1 + A_1(s) + A_2(s) + \cdots + A_m(s)$, where x_1 is the (approximation to the) new point on the orbit, $A_1(s)$ is an n-dimensional vector of polynomials of degree 1 in s which are the first order terms of the Taylor series of $\Phi(t_0, x_0; h)$ at x_0, $A_2(s)$ contains the second order terms, and so on. In this way we compute a numerical approximation to high-order variationals of the flow by computing high-order derivatives of the numerical integration algorithm. A natural question is about the difference between this result and the exact integration of the corresponding variational equations. In particular, if the error is higher for high-order derivatives. This will be useful to design a step size control that takes into account that the numerical integration has been overloaded with jet transport. This is the goal of the next section.

3 Variational flow and jet transport

Consider a generic Initial Value Problem (IVP),

$$\dot{x} = f(t, x), \qquad x(t_0) = x_0, \tag{4}$$

where f is smooth and x belongs to a suitable domain of $\mathbb{R}^n$. We want to compare the results of using jet transport on a numerical integrator for this equation and the results obtained by integrating the corresponding variational equations with the same numerical integrator. In this comparison, we restrict ourselves to Runge-Kutta methods (explicit or implicit), Taylor method and multistep methods. The main result is given by the next theorem.

Theorem 3.1. *Given a step size h, the use of jet transport of order m on a Runge-Kutta method, Taylor method or multistep method produces exactly the same results as the integration of variational equations up to order m with the same method.*

Proof. First, we will show in the following subsections (Propositions 3.2 and 3.3) that the use of jet transport of order 1 on a Runge-Kutta or Taylor method for (4) produces exactly the same results as the ones obtained by using this numerical integrator on the first order variational equations,

$$\begin{aligned} \dot{x} &= f(t, x), & x(t_0) &= x_0, \\ \dot{v} &= D_x f(t, x) v, & v(t_0) &= v_0, \end{aligned} \tag{5}$$

where $v(t) \in \mathbb{R}^n$ and $v_0 \neq 0$ is an arbitrary direction. Then, the proof of the theorem is easily completed proceeding recurrently on m: note that the variational flow of (5) contains the second variational flow of (4) so we can use the previous proposition to show that the result is true up to second order variational equations, and so on. The proof for the multistep method is very similar to the proof for the Runge-Kutta case and we omit the details. □

To describe the numerical methods in this section we use the notation

$$\dot{y} = F(t, y), \qquad y(t_0) = y_0, \tag{6}$$

to refer either to IVP (4) or (5). To simplify the presentation, we assume that F is smooth enough on a suitable domain. We will focus on a single (time) step of the methods, using a given time step h. Once it is shown that the jet transport results and the results of integrating the variational flow are equal, it is clear that if we apply the same step size control strategy to both methods we also obtain the same step sizes for the integration.

3.1 Runge-Kutta methods

A generic σ-stage Runge-Kutta method for the IVP (6) is defined by the formulas (see, for instance, [But87, HNW00]),

$$\begin{aligned} &\kappa_i = F(t_0 + c_i h, y_0 + h(a_{i,1}\kappa_1 + \cdots + a_{i,\sigma}\kappa_\sigma)), \quad i = 1, \ldots, \sigma, \\ &y_1 = y_0 + h(b_1\kappa_1 + \cdots + b_\sigma\kappa_\sigma), \end{aligned} \tag{7}$$

where a_{ij}, b_j and c_j are suitable real coefficients and h is the time step. It is well known that, if h is small enough, these equations have a unique solution ([HNW00]). When $a_{ij} = 0$ for $i \leq j$ the method is explicit, which means that the vectors κ_j can be obtained explicitly.

The goal of this section is to show that to use jet transport of order 1 on the σ-stage Runge-Kutta method (7) to approximate the solution and the variational flow of (4) is exactly the same as to apply the Runge-Kutta method (7) to the IVP (5). To this end, let us introduce the following notation. Let us denote the values κ_j that corresponds to the IVP (5) as $\kappa_j = (\bar{\kappa}_j, \hat{\kappa}_j)$ where $\bar{\kappa}_j$ refers to the coordinates x, and $\hat{\kappa}_j$ refers to the coordinates v.

Proposition 3.2. *Assume that we are using jet transport of order 1 on the scheme* (7) *when applied to the IVP* (4)*. Then, the κ_j values obtained are exactly $\bar{\kappa}_j + \hat{\kappa}_j s$.*

Proof. If we use jet transport of order 1 on a Runge-Kutta method applied to the IVP (4) we obtain the equations

$$\bar{\kappa}_i' + \hat{\kappa}_i' s = f(t_0 + c_i h, x_0 + v_0 s + h \sum_{j=1}^{\sigma} a_{i,j}(\bar{\kappa}_j' + \hat{\kappa}_j' s)).$$

This equation is equivalent to

$$\bar{\kappa}_i' + \hat{\kappa}_i' s = f(t_0 + c_i h, x_0 + h \sum_{j=1}^{\sigma} a_{i,j}\bar{\kappa}_j') + D_x f(t_0 + c_i h, x_0 + h \sum_{j=1}^{\sigma} a_{i,j}\bar{\kappa}_j')(v_0 + h \sum_{j=1}^{\sigma} a_{i,j}\hat{\kappa}_j')s,$$

which implies

$$\begin{aligned} \bar{\kappa}_i' &= f(t_0 + c_i h, x_0 + h \sum_{j=1}^{\sigma} a_{i,j}\bar{\kappa}_j'), \\ \hat{\kappa}_i' &= D_x f(t_0 + c_i h, x_0 + h \sum_{j=1}^{\sigma} a_{i,j}\bar{\kappa}_j')(v_0 + h \sum_{j=1}^{\sigma} a_{i,j}\hat{\kappa}_j'). \end{aligned}$$

These are the equations (7) for $\kappa_j = (\bar{\kappa}_j, \hat{\kappa}_j)$ corresponding to the IVP (5). As the solution is unique ([HNW00]), we have that $\bar{\kappa}_j = \bar{\kappa}_j'$, $\hat{\kappa}_j = \hat{\kappa}_j'$. □

This implies that a single step of a RK method (either explicit or implicit) with jet transport of order 1 on (4) produces the same result as a single step of the RK on (5).

3.2 Taylor method

One of the oldest methods for the numerical integration of an IVP like (6) is based on the computation of the Taylor series of the solution.

$$y_1 = y_0 + y_0^{[1]}h + y_0^{[2]}h^2 + \cdots + y_0^{[p]}h^p,$$

where $y_0^{[i]}$ denotes the normalized derivative of the solution of (6) at t_0,

$$y_0^{[i]} = \frac{1}{i!}\frac{d^i y}{dt^i}(t_0).$$

The computation of the values $y_0^{[i]}$ by taking derivatives to both sides of the ODE can be a difficult process and, moreover, it produces very complex expressions for these derivatives so that the resulting method is not very efficient, specially if high orders are required. On the other hand, automatic differentiation can be used to compute these normalized derivatives very efficiently, up to high orders, giving rise to very efficient implementations of Taylor method ([JZ05]). As before, we can use jet transport on the Taylor method to approximate the variational flow. This has been implemented in the new version of the package `taylor`, [GJZ22].

Proposition 3.3. *A step of Taylor method with first order jet transport on the IVP* (4) *produces exactly the same results as a step of Taylor method on the IVP* (5).

Proof. The i-th normalized derivative of the orbit of (5) is

$$x_0^{[i]} = \frac{1}{i!}\frac{d^{i-1}}{dt^{i-1}}[f(t,x(t))](t_0,x_0), \qquad v_0^{[i]} = \frac{1}{i!}\frac{d^{i-1}}{dt^{i-1}}[D_x f(t,x(t))](t_0,x_0)v_0,$$

which can be used to perform a Taylor step on (5).

To apply jet transport of order 1 to (4), we replace x_0 by $x_0 + v_0 s$ and we propagate first derivatives with respect to s,

$$\begin{aligned}
&\frac{1}{i!}\frac{d^{i-1}}{dt^{i-1}}[f(t,x(t))](t_0,x_0+v_0s) \\
&\qquad = \frac{1}{i!}\frac{d^{i-1}}{dt^{i-1}}[f(t,x(t))](t_0,x_0) + D_x\frac{1}{i!}\frac{d^{i-1}}{dt^{i-1}}[f(t,x(t))](t_0,x_0)v_0s + O(s^2) \\
&\qquad = \frac{1}{i!}\frac{d^{i-1}}{dt^{i-1}}[f(t,x(t))](t_0,x_0) + \frac{1}{i!}\frac{d^{i-1}}{dt^{i-1}}[D_x f(t,x(t))](t_0,x_0)v_0s + O(s^2) \\
&\qquad = x_0^{[i]} + v_0^{[i]}s + O(s^2).
\end{aligned}$$

That is, the Taylor coefficients obtained from jet transport of order 1 are exactly the same as the Taylor coefficients coming from the variational equations. Hence, given an order and a nonzero time step h, the output of a step of Taylor integration using jet transport of order 1 on (4) gives exactly the same results as using Taylor method on (5). □

Remark 2. Theorem 3.1 is also true for methods (either explicit or implicit) in which the new point on the orbit is found as a linear combination of evaluations of the vector field at given points. We do not include the details since the proofs are very similar to the ones for the Runge-Kutta case.

3.3 Stepsize control

As the use of jet transport is equivalent to the integration of the normalized variational equations[1], we can use the standard stepsize control of the numerical integration. This means that we can use the coefficients of the A_j (see Section 2.4) as if they were the values obtained of the numerical integration of the normalized variational equations. Therefore, applying the stepsize control using these coefficients gives the same result as applying the stepsize control on an integration of the (normalized) variational flow.

In some cases, for instance when we are computing very high-order derivatives, we do not require the same level of accuracy for all of them (sometimes, high-order derivatives require less accuracy than the low order ones). Then, we could use a weighted norm in the stepsize control.

4 Power expansion of Poincaré maps

Assume that we have a flow defined by a smooth ordinary differential equation defined on an open subset of $\mathbb{R}^n$, and that we are using a suitable Poincaré section to study its flow. To simplify the discussion, we will consider two separate cases. One when the section is based on a known time of integration (temporal section) and a second one based on an unknown time but determined by the crossing on a certain region (spatial section).

In what follows, $\Phi(t; t_0, x^{(0)})$ denotes the solution at time t of the initial value problem corresponding to the initial data $(t_0, x^{(0)})$.

4.1 Temporal Poincaré sections

This is a common situation when we have a periodically time-dependent ODE with a period, say, $T > 0$. Then, it is usual to define a Poincaré map P as the time T flow of the ODE, that is, $P(x) = \Phi(T; 0, x)$. Periodic orbits of period T appear as fixed points of P, $P(x^*) = x^*$. The linear stability of the periodic orbit follows from the monodromy matrix $D_x P(x^*)$, but to study nonlinear aspects of the dynamics higher order terms are needed. A typical example is the analysis of bifurcations ([Kuz04]).

The power expansion (up to order m) of P at a given point $x^{(0)} \in \mathbb{R}^n$ can be obtained by evaluating P on $x^{(0)} + s$, using a jet arithmetic of order m for the n-dimensional vector of symbols s.

4.2 Spatial Poincaré sections

To simplify the discussion, we focus on an autonomous ODE in $\mathbb{R}^n$. This is in fact the usual situation in which spatial sections are used. Let us assume (also for simplicity) that the Poincaré section Σ is defined by a plane in general position. Let $x^{(0)}$ be a point on the plane Σ, and let us denote by $\vec{n}$ the normal vector to this plane. We assume that, after some integration time $T(x^{(0)})$, depending on the initial point, the trajectory comes back to the section, i.e. $\Phi(T(x^{(0)}); 0, x^{(0)}) \in \Sigma$. To produce the expansion, we have to define coordinates on the plane. Without loss of generality, let us choose $x^{(0)}$ as the origin of coordinates, and let us choose suitable linearly independent unitary vectors $v_1, \ldots, v_{n-1}$ such that $x^{(0)} + v_1 s_1 + \cdots + v_{n-1} s_{n-1}$ is a parametric representation of Σ.

[1] By normalized variational equations we refer to the variational equations divided by the corresponding factorials so that they are the normalized derivative of the flow.

Now we start the integration of the ODE at the point $x^{(0)} + v_1 s_1 + \cdots + v_{n-1} s_{n-1}$ using a jet arithmetic of order, say, m, with the symbols $s = (s_1, \ldots, s_{n-1})$. Note that if we stop the integration at time $T(x^{(0)})$ what we obtain is the power expansion of the flow at time $T(x^{(0)})$ w.r.t. the $n-1$ variables that are the coordinates on Σ, but this is not the power expansion of the Poincaré map $P\colon \Sigma \to \Sigma$ because this expansion does not lay inside Σ. To produce the power expansion of the Poincaré map up to a given order m, we stress that the time needed for an orbit to return to the section Σ depends on the initial point. This means that the return time also depends on s, that is, we have to write the return time as a formal series on s,

$$T(x^{(0)} + v_1 s_1 + \cdots + v_{n-1} s_{n-1}) = T(x^{(0)}) + \sum_{|k|=1}^{m} \tau_k s^k, \tag{8}$$

whose coefficients τ_k are real numbers that have to be determined from the condition

$$\Phi(T(x^{(0)} + v_1 s_1 + \cdots + v_{n-1} s_{n-1}); 0, x^{(0)} + v_1 s_1 + \cdots + v_{n-1} s_{n-1}) \in \Sigma. \tag{9}$$

As usual, this condition must hold up to order m in s. In other words, we expect that the distance between the evaluation of the power expansion of the Poincaré map and Σ behaves like $O_{m+1}(\|s\|)$. As we will see, the coefficients τ_k in (8) can be computed recurrently, degree by degree. To shorten the following formulas, we denote $T_0 = T(x^{(0)})$ and

$$\bar{s} = v_1 s_1 + \cdots + v_{n-1} s_{n-1}.$$

Let us denote $x^{(1)} = \Phi(T_0; 0, x^{(0)}) \in \Sigma$ and we recall that the ODE is $\dot{x} = f(x)$. Let us start by the degree $m = 1$. The flow at time $t = T_0 + \sum_{|k|=1} \tau_k s^k$ can be written as

$$\begin{aligned}
\Phi(T_0 + \sum_{|k|=1} \tau_k s^k; 0, x^{(0)} + \bar{s}) &= \Phi(T_0; 0, x^{(0)} + \bar{s}) + D_t \Phi(T_0; 0, x^{(0)} + \bar{s}) \sum_{|k|=1} \tau_k s^k \\
&= \Phi(T_0; 0, x^{(0)}) + \sum_{|k|=1} a_k s^k + D_t \Phi(T_0; 0, x^{(0)}) \sum_{|k|=1} \tau_k s^k \\
&= x^{(1)} + \sum_{|k|=1} a_k s^k + f(x^{(1)}) \sum_{|k|=1} \tau_k s^k,
\end{aligned}$$

where the values a_k come from the first order expansion of $\Phi(T_0; 0, x^{(0)} + \bar{s})$ w.r.t. s,

$$\Phi(T_0; 0, x^{(0)} + \bar{s}) = x^{(1)} + \sum_{|k|=1} a_k s^k.$$

Hence, to impose condition (9) at first order (at order 0 is already satisfied) we have to ask that

$$\sum_{|k|=1} \left\langle a_k + \tau_k f(x^{(1)}), \vec{n} \right\rangle = 0,$$

where $\langle \cdot, \cdot \rangle$ denotes the standard scalar product. This condition implies that

$$\tau_k = -\frac{\langle a_k, \vec{n} \rangle}{\left\langle f(x^{(1)}), \vec{n} \right\rangle}.$$

From a geometric point of view, this is equivalent to project the directional derivatives w.r.t. each component of s on the Poincaré section, following the flow (see Figure 1).

The computation of the higher order terms is more involved. In particular, it requires to perform integration steps with step sizes that also depend on $\bar{s}$. This introduces a limitation: if, for instance, we have to perform the step size $h = \sum_{|k|=1} \tau_k s^k$ and the numerical integration has a local truncation error of $O(h^p)$, then the resulting power expansion in s will have an error of the order of $O(|s|^p)$ and this means that we cannot trust the resulting expansion in s for orders equal and higher than p. Therefore, we have to limit the degree of these expansions by the order of the local truncation error of the numerical integration algorithm. We note that this is not a limitation for Taylor methods, since the order can be easily increased to the desired value.

Now let us focus in the computation of high-order derivatives, assuming that the order of the local error is large enough for the derivatives we want to obtain. We proceed in a recurrent way. Assume now that we have computed the values τ_k for $|k| \leq m$, and we want to compute them for $|k| = m + 1$:

$$\begin{aligned}
&\Phi\left(T(x^{(0)}) + \sum_{|k|=1}^{m} \tau_k s^k + \sum_{|k|=m+1} \tau_k s^k; 0, x^{(0)} + \bar{s}\right) \\
&= \Phi\left(T(x^{(0)}) + \sum_{|k|=1}^{m} \tau_k s^k; 0, x^{(0)} + \bar{s}\right) + D_t\Phi\left(T(x^{(0)}) + \sum_{|k|=1}^{m} \tau_k s^k; 0, x^{(0)} + \bar{s}\right) \sum_{|k|=m+1} \tau_k s^k \\
&= x^{(1)} + \sum_{|k|=1}^{m+1} a_k s^k + f(x^{(1)}) \sum_{|k|=m+1} \tau_k s^k.
\end{aligned}$$

To obtain the last equality note that, as $D_t\Phi$ is multiplying $\sum_{|k|=m+1} \tau_k s^k$ which is already of order $m + 1$, we have to use the terms of degree 0 of $D_t\Phi$, that is, $D_t\Phi(T(x^{(0)}); 0, x^{(0)})$ which is $f(x^{(1)})$. Therefore, for $|k| = m + 1$, imposing condition (9) leads to the same expression as before,

$$\tau_k = -\frac{\langle a_k, \vec{n}\rangle}{\langle f(x^{(1)}), \vec{n}\rangle}.$$

Let us summarize how to apply these formulas. We first integrate for a time $T(x^{(0)})$ such that the orbit starting at the initial condition $x^{(0)}$ lands on the Poincaré section Σ. This integration can be done with jet transport so that we obtain $\Phi(T(x^{(0)}); 0, x^{(0)} + \bar{s})$. Then, to compute the return time (8) such that the power expansion of the flow lays inside Σ up to degree m, we proceed degree by degree in (8): for degree 1, we use first the formulas above to compute the numbers τ_k, and then we perfom a step of numerical integration with step

$$h = \sum_{|k|=1} \tau_k s^k, \tag{10}$$

starting at $\Phi(T(x^{(0)}); 0, x^{(0)} + \bar{s})$ to obtain $\Phi(T(x^{(0)}) + \sum_{|k|=1} \tau_k s^k; 0, x^{(0)} + \bar{s})$ which is a power expansion with its first order terms inside Σ. Next, using the second order terms w.r.t s in $\Phi(T(x^{(0)}) + \sum_{|k|=1} \tau_k s^k; 0, x^{(0)} + \bar{s})$ (the coefficients of these terms are the values a_k above) we compute the values τ_k for $|k| = 2$ and we perfom another numerical integration step,

$$h = \sum_{|k|=2} \tau_k s^k, \tag{11}$$

starting at $\Phi(T(x^{(0)}) + \sum_{|k|=1} \tau_k s^k; 0, x^{(0)} + \bar{s})$ to obtain $\Phi(T(x^{(0)}) + \sum_{|k|=1}^{2} \tau_k s^k; 0, x^{(0)} + \bar{s})$ with its second order terms inside Σ. This process is continued up to the desired order. Figure 1

illustrates these ideas. Another approach is to consider a Newton approach to find the τ_k in (8) imposing the condition on (9) , see [Sim90].

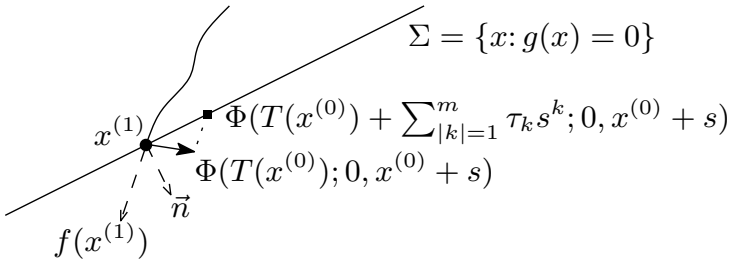

Figure 1: Projection of a directional derivative of the flow on the Poincaré section.

It is important to note that, in this procedure, the truncation error of the time stepper can affect to the jets. For instance, if we use a time stepper with a local truncation error of the form $O(h^{p+1})$, after a step of the form (10) or (11), the error of the numerical integration contains terms of order $p+1$ in s and, therefore, it is impossible to obtain derivatives of the spatial Poincaré map of order higher than p. So, if high order derivatives are wanted, it is better to use a numerical integration method like the Taylor method, where it is very easy to obtain a high order truncation error.

4.3 On normal forms

One of the applications of the power expansion of a Poincaré map is the computation of normal forms. A normal form is a local (and high order) integrable approximation of the dynamics in a neighborhood of an invariant object like a fixed point or an invariant curve, and it is useful to have accurate information of the nearby dynamics [DJ22]. So, it is possible to use the machinery in this paper to compute high order normal forms [GJJC$^+$].

5 The parametrization method

The origin of the parametrization method goes back to the 80's when it was used by C. Simó (see also [FR81]) for numerical computations. It is remarkable that this method is also excellent to prove the existence of invariant manifolds, as shown by X. Cabré, E. Fontich and R. de la Llave [CFdlL05]. Here, we are only interested in computing these invariant manifolds from an algorithmic point of view. A complete description of the method can be found in the book [HCL$^+$16].

Let P be a Poincaré map. To discuss the paremetrization method for invariant manifolds, let us first focus on the case for which the manifold is unstable. The stable one can be computed similarly replacing P by P^{-1}. In the case that P is given in terms of a flow map, its inverse is obtained integrating the differential equation backwards in time (see [GJNO22] for more details). The main idea of the method is to consider that the manifold can be parametrized by a map K which we denote as a formal power series. Then K is plugged into the invariance equation involving K, P, and internal dynamics of the manifold. Thus, each term of the formal series can be solved order by order. You will note that, as far as the final series is converging, the map K will be unique up to a scaling factor. We assume:

- There exists a fixed point z_0 by the map P, i.e. $P(z_0) = z_0$,

- there exists a decomposition $\mathbb{R}^n = \Lambda_u \oplus \Lambda_c \oplus \Lambda_s$, where $\dim(\Lambda_u) = d$ and $\dim(\Lambda_s) = r$. Here Λ_u is the eigenspace corresponding to the d unstable eigenvalues $\lambda_u = (\lambda_1, \ldots, \lambda_d)$ of the matrix $DP(z_0)$. Similarly, Λ_s and Λ_c are the eigenspaces related to the unstable eigenvalues and the elliptic eigenvalues. For the sake of simplicity, we assume that all these eigenvalues are real. The complex eigenvalue case can be handled similarly.

Assume that the parametrization, with parameters $u = (u_1, \ldots, u_d)$, is given by

$$K(u) = \sum_{m \geq 0} A_m, \qquad \text{with} \quad A_m = \sum_{|k|=m} a_k \; u^k, \tag{12}$$

where $k = (k_1, \ldots, k_d) \in \mathbb{N}^d$, is a multi-index, $|k| = k_1 + \cdots + k_d$, $u^k = u_1^{k_1} \cdots u_d^{k_d}$, and $a_k \; u^k$ are the different monomials of degree $|k| = m$. The invariance equation characterizes the invariant manifold –parametrized by the map K– under the dynamics. It is given by

$$P \circ K = K \circ U, \qquad U = \operatorname{diag}(\lambda_1, \ldots, \lambda_d), \tag{13}$$

which we will solve it, order by order, recursively.

The zeroth order is set by the coordinates of the fixed point z_0, i.e. $A_0 = z_0$. The next order has the form $A_1 = \sum_{j=1}^{d} v_j \; u_j$, where $\{v_j\}_{1 \leq j \leq d}$ are the eigenvectors of the matrix $DP(z_0)$ corresponding to the eigenvalues $\{\lambda_j\}$. This choice verifies the invariance equation at first degree order but we have a freedom by scaling the parameters u leading to an equivalent result. Although they are equivalent, a suitable rescaling of the parameters allows to improve the numerical behavior of the series, see Section 5.1.

To compute the next degree orders, we proceed inductively order by order. Assume we have computed the coefficients of A_m up to degree j. Then we can write the series at degree $j+1$ by $K_j(u) + A_{j+1}$, where A_{j+1} must be determined and

$$K_j(u) = \sum_{m=0}^{j} A_m, \qquad \text{with} \quad A_m = \sum_{|k|=m} a_k \; u^k.$$

By applying the invariance condition (13), an expression to A_{j+1} is deducted:

$$\begin{aligned} P(K_j(u) + A_{j+1}) &= P \circ K_j + DP(z_0) A_{j+1} + \mathcal{O}(u^{j+1}) \\ &= K_j \circ U + B_{j+1} + DP(z_0) A_{j+1} + \mathcal{O}(u^{j+1}). \end{aligned}$$

Here B_{j+1} is the Taylor term of order $j+1$ of $P(K_j(u))$ which is obtained following the jet transport technique described in Section 4. To be more precise, it has the form

$$B_{j+1} = \sum_{|l|=j+1} b_l \; u^l. \tag{14}$$

Neglecting the term $\mathcal{O}(u^{j+1})$ and imposing that the last equation has to be equal to $K_{j+1} \circ U$, we get

$$B_{j+1} + DP(z_0) A_{j+1} = A_{j+1} \circ U.$$

Then, for l such that $|l| = j+1$ is given by solving the linear systems

$$\big(DP(z_0) - \lambda_u^l I_n\big) a_l = -b_l, \tag{15}$$

and then,

$$A_{j+1} = \sum_{|l|=j+1} a_l \; u^l,$$

is the homogeneous polynomial of degree $j+1$ we are looking for.

Note that from the computational point of view, the step consisting in getting (14) is, by far, the most expensive step when the computation of P requires to integrate an ODE. Also note that (15) is assumed to be a solvable linear system for each of the different values of l. Those conditions for which the linear systems have a solution are called non-resonance conditions and, in such cases, the manifold admits the locally convergent power series of the form in (12).

Remark 3. Some modifications are convenient when this method is applied in combination with a multiple shooting method, where the map P is split as the composition of several maps. An exhaustive explanation can be found in [GJNO22] in the context of the parametrization of invariant manifolds of high-dimensional tori.

5.1 Scaling factor

The parametrization of the invariant manifold is not unique. In particular, if $K(u)$ is a parametrization in (13), then $K(cu)$ for $c \neq 0$ is also a parametrization. An effect of c is to rescale the coefficients a_k in (12) as $c^k a_k$. In some situations, to minimize the error propagation, we want to avoid the norms of the coefficients to grow or decrease too fast with $|k|$ [Ric80, FdlL92].

If the radius of convergence w.r.t. u in (12) is known, ρ, we can use the scaling $c = \rho$, which scales the radius of convergence to 1 and, hence, gives a mild increasing or decreasing of the size of the coefficients. If the radius of convergence is not known, it can be estimated using, for instance, a root test. If this estimation of the radius ρ_k and the scaling is done at each degree k of the manifold computation, then the scaling factor at each degree k is ρ_k/ρ_{k-1} with $\rho_1 = 1$.

Note that, one may consider to perform the scaling after the end of the parametrization up to a fixed degree, however, to undo and do scaling at each degree is computationally more efficient and it helps the integration of the high-order variational flows since the magnitudes involved are of similar order.

5.2 On the choice of the degree

A numerical implementation of the explained parametrization method in truncating the formal power series (12) up to a certain degree. As the power expansion is computed degree by degree, a criterion to select the final degree consists in estimating, for each degree, the validity region of the parameter u. This is the set of values of u for which the truncated power expression is an accurate representation of the manifold. Assume that we know the coefficients up to degree m, then an estimation of the validity region of the variable u with tolerance ϵ consists in finding a real positive number s, say $s_m^{\max}$, such that

$$\sum_{|k|=m} |a_k| \; s^m < \epsilon, \qquad |s| \leq s_m^{\max}. \tag{16}$$

Equation (16) is a rough bound of valid parameters u but it is easily solvable. Indeed, so we can take $s_m^{\max} = (\epsilon / \sum_{|k|=m} |a_k|)^{1/m}$.

To prevent the effect of symmetries (i.e., to deal with the situation when all the coefficients of odd or even degree are zero) we can consider the minimum value of $s^{\max}$ obtained from degrees

m and $m-1$. This computation can be done after the calculation of each degree to decide if this is enough. Hence, a suitable degree choice m is when, for instance, the gain between and $s_m^{\max}$ and $s_{m-2}^{\max}$ has little significance, for example when $s_m^{\max}/s_{m-2}^{\max}$ is below 1.01 or 1.001.

Note that there are, of course, other ways to estimate a validity region of u but they must be computationally easy enough to perform it at each new parametrization degree.

5.3 Globalization

The parametrization K is valid in a neighborhood of the fixed point. To extend the manifold outside this domain we can use a suitable mesh of points on the fundamental interval, and to iterate these points (forward for an unstable manifold, backward for a stable one) to extend the manifold outside this domain. To estimate the error propagation in these iterations we can accumulate, for each point in the fundamental interval, the products of the norms of the differential of the map along each orbit to have an estimate of the error growth factor. When this factor is larger than some prescribed threshold, the globalization should stop. These ideas can be easily extended to globalize higher dimensional manifolds.

6 Examples

In this section, we provide several examples in which we apply the parameterization method as explained in Section 5 to compute high order approximation of stable/unstable manifolds. Those examples are intended to illustrate different situations: In Section 6.1, we globalize the stable and unstable manifolds related to hyperbolic periodic orbits of the Hénon-Heiles system. To do so, a suitable spatial Poincaré section is used. In this example, we take advantage of the high-order approximation to the stable/unstable manifolds to globalize numerically them using fewer iterates of the map. The numerical integration in this example is done my means of a Taylor method. Its variable order allows to compute easily high order derivatives of the Poincaré map, see Section 4.2.

As example, in Section 6.2, we consider a pendulum with a fast periodic forcing. When the perturbation is activated, the system ceases to be integrable and the homoclinic connection of the hyperbolic equilibrium point splits, leading to chaotic behavior of the system. It is well known that, in this situation, the splitting angle is exponentially small with the size of the perturbation. This means that, if the angle is to be computed, extended precision is required. In this example we compare the efficiency between a linear approximation and a high order one when computing the splitting angle. The numerical integrations are done by means of a Taylor method.

In Section 6.3 we compute high-order approximations of the stable/unstable manifold of the dynamical equivalent of the triangular point L_4 in the Bicircular Problem. This dynamical equivalent is a hyperbolic periodic orbit which is mildly unstable. Therefore, to globalize its stable/unstable manifolds starting from a linear approximation, a large number of iterates to move away from the periodic orbit is needed. Here we show that the the parameterization method produces a power expansion of the manifold which is valid in a quite large domain. In this example, the numerical integration is done by means of a Runge-Kutta-Fehlberg 7(8) method. As we are using a temporal (stroboscopic) Poincaré section, the order of the Runge-Kutta does not limit the order of the computed derivatives.

Finally, Section 6.4 deals with a system that models the behavior of an electron near an atomic core and excited by a laser field. Some trajectories, the recolliding orbits, are of especial

interest. These orbits get expelled from the ionic core and come back after some laser cycles. Some of these recolliding trajectories are driven by a hyperbolic periodic orbit which has two unstable directions: One strongly unstable and the other one mildly unstable. Our interest is in computing the 2-dimensional unstable manifold. Notice that the fact that the two hyperbolic eigenvalues are so different in size, brings numerical difficulties to the computation. Therefore, a combination of a high order approximation to the manifold with extended precision arithmetic is required.

6.1 The Hénon-Heiles system

The Hénon-Heiles (HH) system is a Hamilonian model proposed by Michel Hénon and Carl Heiles for the motion of massless star under the attraction of an effective potential due to other stars in a galaxy. The dynamics of the system, of two degrees of freedom, is determined by the Hamiltonian function

$$H = \frac{1}{2}(p_x^2 + p_y^2) + \frac{1}{2}(x^2 + y^2) + x^2 y - \frac{y^3}{3}.$$

The HH system stands out as a classical and simple example of chaotic conservative system. A typical approach to study it, is to consider a certain Poincaré map (e.g. $\{x = 0\}$). Then, the dynamics can be described by means of a family of Area Preserving Maps (APM) parametrized by the energy. When the energy is chosen to be very small, most of the phase space is populated by invariant curves carrying quasi-periodic motion. In a typical converse KAM picture, these invariant curves get destroyed (according to some arithmetic properties of their rotation number) when the value of the energy is increased and the gaps left are occupied by chaotic motion. The destruction of the invariant curve is related to the existence of hyperbolic periodic orbits and their (stable and unstable) invariant manifolds. These manifolds intersect in a complicated tangle in the phase space. The size of the chaotic motion depends on the angle of the intersection, the so called splitting angle. In the case of the family of APM coming from the HH Hamiltonian, these angles are quite large and can be computed easily by using a standard double precision arithmetic.

As example, we have computed some periodic orbits and their stable and unstable manifolds. We used a Taylor integrator [JZ05] with 10^{-16} integration tolerance and modified to work with jet arithmetic, [GJZ22]. The hyperbolic fixed points of the Poincaré map with section $\{x = 0\}$ and fixed Hamiltonian level $H = 0.125$ are reported in Table 1.

	y	p_y	λ_u
q_1	3.01400650333283e-01	2.99870268931536e-01	3.76068592161369
q_2	-1.85405087090801e-01	5.30699126253682e-15	3.76068592161372
q_3	3.01400650333287e-01	-2.99870268931531e-01	3.76068592161374

Table 1: Periodic orbits of HH and its unstable eigenvalue λ_u, being the stable one $1/\lambda_u$.

For each of the points q_ℓ in Table 1, we compute a parametrization of the invariant manifold associated to λ_u and also to $\lambda_s = 1/\lambda_u$ (in this case using the inverse of the Poincaré map) up to the degrees reported in Table 2. These degrees where determine following the strategy described in Section 5.2. The Table 2 also shows the scalings based on estimating the radius of convergence, see Section 5.1, and the validity region of the parametrization with a tolerance 10^{-14} in (16), see Section 5.2. As we can inference from Figure 2 both quantities converge as the degree increase.

	degree	scaling, c	validity region, $s^{\max}$	time (in sec.)
$W^s(q_1)$	66	7.825189525522893e-01	4.776699128424906e-01	10.471215
$W^u(q_1)$	44	2.301773423837667e-01	1.090485567028463e-01	13.105170
$W^s(q_2)$	88	5.097743807635171e-01	3.519317633442122e-01	54.432266
$W^u(q_2)$	88	5.097743807635167e-01	3.519317633442118e-01	54.484148
$W^s(q_3)$	44	2.301773423837770e-01	1.090485567028529e-01	13.105150
$W^u(q_3)$	66	7.825189525522871e-01	4.776699128424852e-01	10.537275

Table 2: Degree, scaling, validity region, and computational time of stable and unstable invariant manifolds for the periodic orbits q_ℓ of HH with Hamiltonian level 0.125.

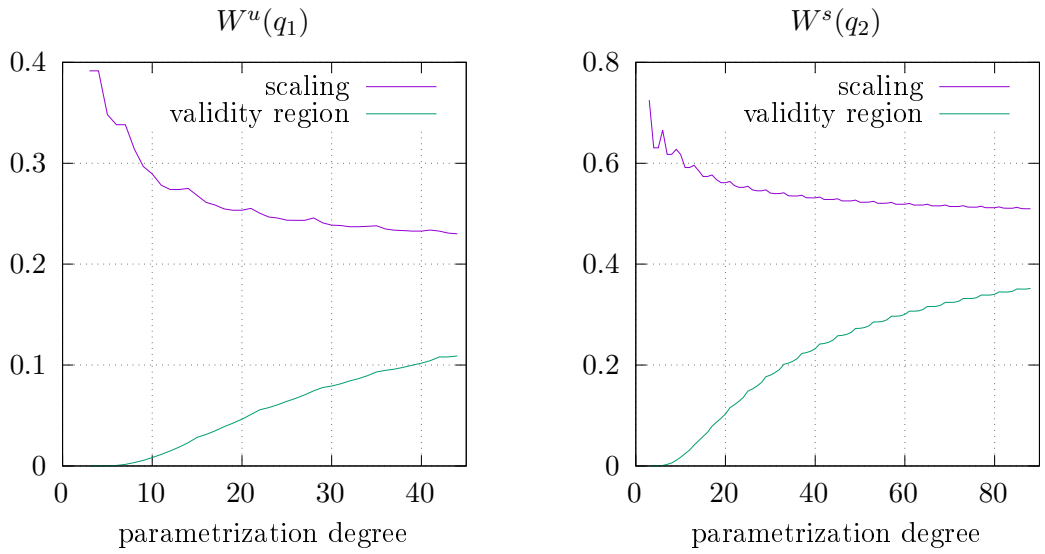

Figure 2: Evolution of the scaling and estimated validity region of the unstable manifold of q_1 and the stable manifold of q_2 in terms of the parametrization degree.

Figure 3 shows the image of the validity range by the Poincaré map done by evaluating the parametrized Taylor expansion for different values of s. The Figure 3 also shows the globalization of the invariant manifolds, following Section 5.3, until the iteration threshold of 10^{12} with the Fröbenius norm. Each of the globalizations took around 40 seconds, and 7 or 8 iterations of the fundamental interval with 10^4 equispaced points in it.

6.2 Splitting of separatrices of a pendulum

Let us consider a model for a rapidly forced pendulum,

$$\begin{aligned} \dot{x} &= y, \\ \dot{y} &= -\sin x + \mu \sin \frac{t}{\varepsilon}. \end{aligned} \tag{17}$$

Here, $0 < \varepsilon < 1$ and μ are small parameters and x is an angular variable (defined $\bmod 2\pi$) so the phase space is topologically a cylinder. The unperturbed ($\mu = 0$) equation has a simple behavior. It has two equilibrium points; an elliptic one at $(0, 0)$ and another one at $(\pm\pi, 0)$ which

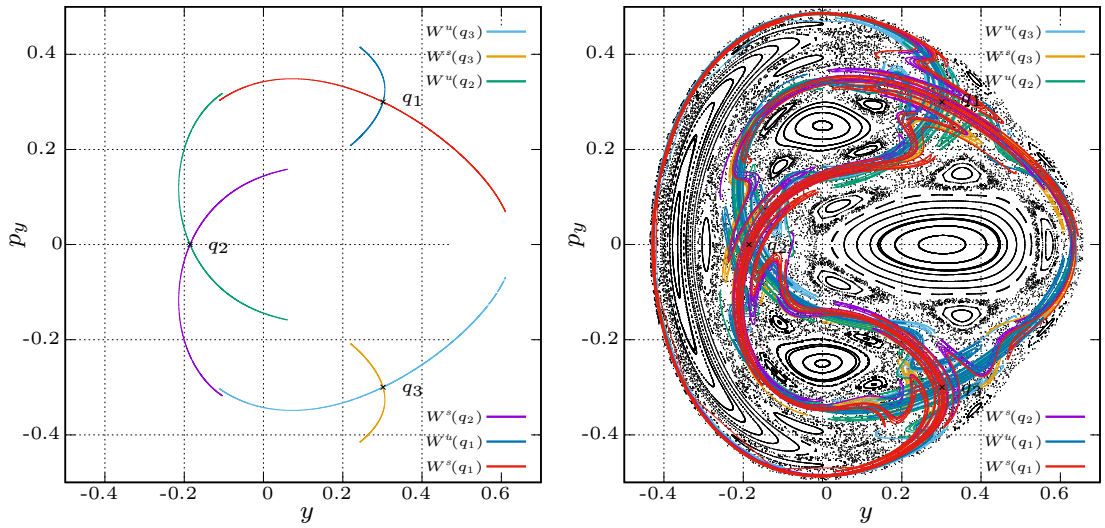

Figure 3: On the left the intervals $[-s_{max}, s_{max}]$ and on the right globalization of the un/stable manifolds overlapping with background the Poincaré plot with Hamiltonian level 0.125.

is hyperbolic. The remaining trajectories are integral curves (the system is integrable, as it has one degree of freedom). These curves are classified in three types: librational (homotopically trivial), rotational (homotopically non-trivial), and separatrices which separate the libration and the rotational curves. The separatrices correspond to the (un)stable invariant manifold associated to the hyperbolic point. That means that the origin is a homoclinic point. As the system is integrable, the stable and unstable manifold coincide (see Figure 4, left). The two homoclinic orbits can explicitly be parameterized as $\Gamma_\pm = \{(x_0(t), \pm y_0(t))\}$, where

$$x_0(t) = 2\arctan(\sinh t),$$
$$y_0(t) = \dot{x}_0(t) = \frac{2}{\cosh t}.$$

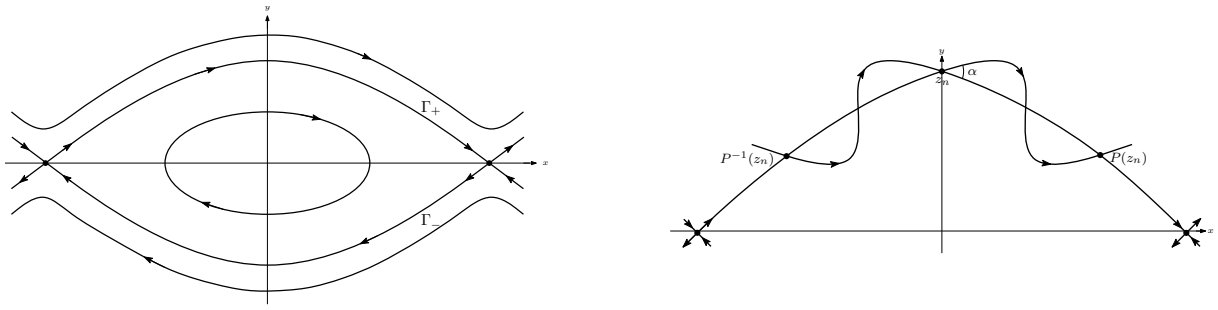

Figure 4: Sketch of the pendulum phase space; in the unperturbed case (left)the (un)stable manifolds coincide while in the perturbed one (right) intersect transversally.

The situation is different when $\mu \neq 0$. First, the system is no longer autonomous but periodic time dependent: Henceforth, the phase space dimension increases by one. Moreover the equilibrium point no longer exist. Using the Implicit Function Theorem, it can be proved that,

for sufficiently small values of μ, the equilibria are replaced by periodic orbits of period $T = 2\pi\varepsilon$ (these are usually called dynamical equivalents). A suitable tool to cope with periodically time dependent systems is the stroboscopic map which is obtained by evaluating the flow at the period: $P(x, y) = \varphi(0, T; x, y)$ and φ stands for the flow of the ODE. Periodic orbits of period T are fixed points of P. Since in this example the system is Hamiltonian, the map will be symplectic. Again, if μ is small enough, the dynamical equivalent of the origin is a hyperbolic fixed point of P and, therefore, there exist stable/unstable manifolds attached to the fixed point. Another consequence of the perturbation is that the system is no longer integrable, therefore the manifolds do not coincide, but they intersect infinitely many times, producing a homoclinic tangle. Due to the symmetries of the system, these manifolds are forced to intersect at the vertical axis (see Figure 4, right). The angle α in the intersection of the manifolds provides insight on the chaotic motion near the separatrices. In particular, if $\alpha \neq 0$, the invariant manifolds intersect transversely and this leads to regions of chaotic motion. This angle can be studied asymptotically as the next result shows:

Theorem 6.1 ([DS92])**.** *For $\varepsilon \to 0$ and $\mu \to 0$, the following asymptotic formula hold.*

$$\alpha = \frac{\pi}{2\varepsilon} \frac{\mu}{\cosh \frac{\pi}{2\varepsilon}} \left[1 + O(\mu, \varepsilon^2)\right]. \tag{18}$$

In this section we will discuss the numerical computation of this exponentially small intersection angle, stressing the huge advantages provided by the use of high-order variational flow, especially when high accuracy is needed. To this end, we have chosen the MPFR library ([FHL+07]) that allows the user to select the number of digits and has proven to be efficient and reliable. To use it from a C program we have "updated" it to C++ to use the operator overload facility of this language to replace the standard double precision of the computer with MPFR.

Before starting with the computations, note that the symmetries of the Hamiltonian imply that it is enough to compute the angle of intersection α^* of the manifold with the vertical axis $\{x = 0\}$: the splitting angle is then $\alpha = 2\alpha^*$ (note that $\alpha^* = 0$ means that the manifold is perpendicular to $x = 0$). So, in what follows, we will compute α^*. To this end we first compute the hyperbolic point by a standard Newton method, then we produce an approximation of the manifold and we globalize it till it intersects $x = 0$. The goal here is to compare the performance of the method when the approximation of the manifold is linear against a high order approximation. Independently of the approximation, a way to obtain the splitting angle is as follows:

1. We select a fundamental domain J of the manifold, close enough to the fixed point so the approximation of the manifold is valid with a fixed accuracy.

2. We compute m such that $P^m(J)$ crosses the vertical axis $\{x = 0\}$. Notice that the fundamental domain J can be chosen to be far away of the fixed point if the approximation of the manifold is of high order and, therefore, m will be smaller in that case.

3. We compute the parameter $s^* \in J$ for which $P^m(K_u(s^*))$ is on the vertical axis $\{x = 0\}$ at a point $y = y_*$.

4. We approximate, by means of numerical differentiation, the tangent vector of the manifold at $(0, y^*)$.

5. Using the tangent vector, we compute α^*.

One of the inconveniences one has to overcome with this computation is the accumulation of error. Indeed, close to the fixed point, the amplification of error can be estimated by means of the norm of the differential map $DP^m(K_u(s^*))$. As the unstable manifold is attracting at least near the fixed point, it is not difficult to produce a globalization of the manifold. However, in this case we are interested in computing the crossing point of the unstable manifold and the vertical axis. This is a little bit more complicated as the numerical error is also expanded along the stable direction (again, close to the fixed point) so that the error in the evaluation of P^m is large at it does not allow an accurate computation of s^* (for instance, if $\|DP^m(s^*)\| \approx 10^{20}$, then we will loose 20 decimal digits in this computation). Notice also that the amplification factor grows exponentially with the number of iterates and, therefore, it is advisable to keep it small.

We have tested the algorithm for the case $\varepsilon = 1/32$ and $\mu = 1/1024$. As we have already discussed, extended accuracy is required for this computation. Hence, have chosen a Taylor method ([JZ05]) with MPFR arithmetic with mantissa of 65 decimal digits. To compute the hyperbolic fixed point of P near $p_h = (-\pi, 0)$ we request $P(x, y) - (x, y) = 0$, using a Newton method with initial condition p_h. In Table 3 we display the coordinates of the fixed point, the unstable eigenvalue, and the related (normalized) eigenvector. We have computed the splitting for both the linear approximation of the manifold and an approximation of order 32. In Table 4 we display the results. The splitting angle computed for both cases is approximately $\alpha^* \approx 1.452038838722046 \times 10^{-23}$. Notice that, the amplification factor in the case of the linear approximation is of order 10^{32} and this implies that the linear approximation only allows to compute the splitting angle with accuracy of about 10^{-33}. This restriction is not present when using the approximation of order 32 for the manifold.

To check the accuracy of each computation, we have ran again the program doubling the number of digits (that is, using a mantissa of 130 digits) and reduced the precision thresholds accordingly. Then, comparing the new splitting angle with the ones computed with the linear approximation and with the approximation of order 32 we see that the disagreement of the splitting angle for the linear approximation is of order 10^{-33} while for the approximation of order 32 is of order 10^{-64}. Errors of the same magnitudes are obtained when computing the crossing point at the vertical axis.

Regarding the computation time, there is no penalization in using high order approximation (of order 32). Using 65 digits, to compute the parameterization up to order 32 takes about 11 seconds. The computation of the splitting using this high order parameterization, takes about 7 seconds. The whole process to compute the splitting is, therefore, about 18 seconds. To compute the splitting using the linear approximation takes about 29 seconds.

The optimal degree to use depends on two factors: The computation time and the accuracy. Increasing the degree of the expansion increases the accuracy of the computation and also decreases the computing time of the splitting (once the manifold has already been obtained). However, the computing time devoted to compute the expansion increases remarkably as the order gets high. In Table 5 we display several runs of the program but using different orders and a mantissa of 65 digits. Order 1 corresponds to the linear approximation. The largest order (78) is the last order in which we obtain a significant increase on the radius of convergence (about 1%). The first column of Table 5 displays the order, the second column shows the time (in seconds) needed to compute the expansion of the manifold. In the third column shows the number of necessary iterates to cut the vertical axis in the computation of the splitting. This number is critical in both, accuracy and computing time. The fourth column displays the order of the amplification factor (**OAF**). The amplification factor is of order 10^{OAF}. **OAF** provides

$x =$	-3.14159265358979323846264338327950288419716939937510582097494 5
$y =$	-0.00003048780487804878348741641977273061910125692778654579395 0
$\lambda =$	1.21695220550761317997660218588773509916027624940673711060844 7
$v_x =$	0.70710678118658760124047248750533567611697820126936749788789 2
$v_y =$	0.70710678118650744756121623443291894113642980629050741284498 0

Table 3: Hyperbolic fixed point (x, y), its unstable eigenvalue λ, and its eigenvector $v = (v_x, v_y)$, with 60 digits.

Linear approximation

Iterates	384
Amplif.	2.0734198e+32
Angle	1.45203883872204592210415370294486922293980702030435119188385645 7e-23

High order approximation

Iterates	24
Amplif.	111.31778
Angle	1.45203883836956616271818262378297040966256292145750368528676186 94e-23

Table 4: Number of iterates to cut the vertical axis, amplification factor and splitting angle. Top: Linear approximation. Bottom: Approximation of order 32.

an estimation of the digits lost due to the amplification factor. The fifth column displays the necessary time (in seconds) to compute the splitting (once the expansion is already obtained) and the sixth column displays the total time (in seconds).

The main takeaway of Table 5 is that we can avoid the propagation of errors due to the amplification factor if we go to order 78. Nevertheless, the computation time is exceeds the computation time using the linear approximation (149 seconds vs. 29 seconds). Going up to order 50 takes about 44 seconds to obtain the splitting loosing just one digit. The best results (counting accuracy and computation time) are obtained for orders 16 and 20 (In both cases take about 13 seconds to compute the splitting losing 3 digits). Going up to order 32 provides better accuracy (losing 2 digits) for 18 seconds of computing time. Finally, going to order 8 and 12 takes about 22 and 17 seconds respectively but more digits are lost (7 and 5). Most of the computing time for these two cases is spent in computing the splitting, as the expansions take less than a second. Notice the dramatic gain in accuracy from going to linear approximation (losing 32 digits) to order 8.

6.3 The unstable manifold of L_4 in the Bicircular Problem

In celestial mechanics, the (Earth-Moon) Bicircular Problem (BCP) is a common problem which comes from a restricted version of the Four Body Problem [Hua60, CRR64]. In suitable coordinates, this model is a perturbation of the well known Restricted Three Body Problem (RTBP), see [Sze67]. The Earth-Moon BCP assumes that the Sun and the Earth-Moon barycentre move along a circular orbit around the center of mass of the Sun-(Earth+Moon) system while Earth and Moon move as in the RTBP. While written in the standard units and (synodic) coordinates of the RTBP, the BCP is a periodic time dependent perturbation of the RTBP. The perturbation

Order	TM (s)	It	OAF	TS(s)	Total(s)
1		384	32	29	29
8	<1	84	7	21	<22
12	<1	59	5	16	<17
16	1	45	3	12	13
20	3	37	3	10	13
32	11	24	2	7	18
50	40	16	1	4	44
78	146	11	0	3	149

Table 5: Metrics for the computation of the splitting using different orders and a mantissa of 65 digits. The columns display the order, the time in seconds to compute the expansion of the manifold (**TM(s)**), the number of iterates to compute the splitting (**It**), the order of the amplification factor (**OAF**), the time in seconds to compute the splitting with the manifold already expanded (**TS(s)**) and the total time in seconds respectively.

preserves the Hamiltonian structure of the RTBP and its Hamiltonian function is

$$H_{BCP} = \frac{1}{2}(p_x^2 + p_y^2 + p_z^2) + yp_x - xp_y - \frac{1-\mu}{r_{PE}} - \frac{\mu}{r_{PM}} - \frac{m_S}{r_{PS}} - \frac{m_S}{a_S^2}\big(y\sin\theta - x\cos\theta\big). \quad (19)$$

where m_S is the mass of Sun, a_S the semi-major axis of Sun, $r_{PE}^2 = (x-\mu)^2 + y^2 + z^2$, $r_{PM}^2 = (x-\mu+1)^2 + y^2 + z^2$, $r_{PS}^2 = (x-x_S)^2 + (y-y_S)^2 + z^2$, $x_S = a_S\cos\theta$, $y_S = -a_S\sin\theta$, $\theta = \omega_S t$ and ω_S is the mean angular velocity of Sun in the synodic coordinates.

μ	0.012150581623433623
m_S	328900.55
a_S	388.81114302335106
ω_S	0.92519598551829646

Table 6: Values of the parameters for the BCP used in this work.

In the BCP the Lagrangian points are no longer equilibria, they are replaced by periodic orbits with the same period as the perturbation: $T_S = 2\pi/\omega_S$. In particular, the triangular point L_4 is replaced by three periodic orbits of period T_S, see [SGJM95, CJ00, JCFJ18]. One of these orbits is slightly unstable, of linear type saddle×center×center. This unstable periodic orbit is seen as an hyperbolic fixed point of the stroboscopic map (the map obtained evaluating the flow at the period T_S) has an unstable eigenvalue close to 1.098. Notice that this instability is remarkably mild, that is, an initial condition on the manifold near to the fixed point needs a large number of iterates to get far from it. Therefore, to grow numerically the manifold from the linear approximation is numerically expensive. We can, however, produce a high-order approximation of the manifolds and produce large pieces of the manifolds that can be mapped a few times to get even larger pieces of the manifold, see Figure 5.

Let us give some details on how Figure 5 is produced: First, we modify the well-known Runge-Kutta-Fehlberg 7(8) method [Feh68] to work with a jet arithmetic. Then we apply the parametrization method to obtain, order by order, a Taylor expansion of the manifolds. At each

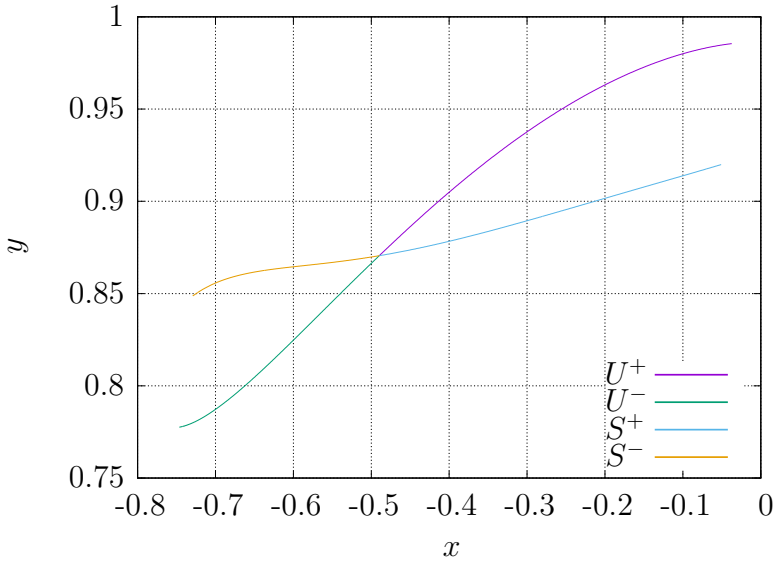

Figure 5: High-order approximations of the stable (S^+, S^-) and unstable (U^+, U^-) manifolds attached to the dynamical equivalent of L_4 in the Earth-Moon BCP.

step, after we compute the coefficient of order k, we use the root criterion to estimate the radius of convergence. Obviously, this radius is increased at each step. When the gain of the radius of convergence is less than 1%, we stop the computation. We denote by U^+ and U^- the two pieces of the unstable manifold, using the above-mentioned criterion, these manifolds are expanded up to order 54. On the other hand, the stable pieces, denoted by S^+ and U^-, are expanded up to order 46. Then, all those Taylor expansions are evaluated to obtain the curves in Figure 5.

6.4 A two-dimensional invariant manifold related to recolliding electrons

In this example, we consider the motion of an electron in an atom that is perturbed by a strong linearly polarized laser field. When the electron is "impacted" by the laser with sufficient energy, it gets expelled out from the atomic core. An interesting question is whether the electron is re-captured by the atom following the Coulomb's laws. This phenomenon is known as recollision. Recollision physics is an emerging field, highly related to collision physics and optics, see [Cor93, Cor14] and it has been tackled from the dynamical systems perspective, see [MCU10, MKCU12, KCUM14, KMCU14, NCUW15, MKCU12] and references therein.

Most of these references, consider the case in which the electron is allowed to move in a line (i.e. the configuration space has dimension one). Here, we consider the two-dimensional configuration space case. It can be modeled as a Hamiltonian system with two degrees of freedom and periodic time dependence written as follows:

$$H = \frac{1}{2}(p_x^2 + p_y^2) - \frac{1}{\sqrt{x^2 + y^2 + 1}} + E_c x \cos(\omega t), \tag{20}$$

where $\omega = 0.0584$ is the frequency of the laser, $E_c = 0.1$ its amplitude. We notice that this Hamiltonian function has three terms: The kinetic energy, the potential energy and the laser interaction. In a neighborhood of the atom core, the laser acts as a periodic perturbation.

As usual, this problem is better faced by means of the stroboscopic map which, we recall, is given by the flow of system (20) evaluated at the period $2\pi/\omega$.

The dynamical mechanism that guide most of the recolliding orbits is well understood when the electrons move in a one dimensional space, that is, the dynamics restricted to the invariant subspace $\{y = 0, p_y = 0\}$ of system (20). The stable and unstable manifolds of some key hyperbolic fixed point drive these trajectories to recollide many times, see [KCUM14]. Notice that a fixed point of the stroboscopic map corresponds to a periodic orbit of period $2\pi/\omega$.

In the two dimensional configuration space, this fixed point does not drive recollisions outside the invariant subspace $\{y = 0, p_y = 0\}$, see [DJCJC22]. The reason is that its normal behavior is of type saddle×saddle. Therefore, the stable and unstable manifolds attached to the fixed point are two-dimensional while the phase space is four-dimensional. This means that the invariant manifold do not separate the phase space as in the one-dimensional case.

The hyperbolic fixed point studied in [KCUM14], is located near $x = 30.5$, $y = p_x = p_y = 0$. This orbit is easily refined by using a Newton method. The eigenvalues of the Jacobian matrix of the stroboscopic map are displayed in Table 7.

λ_1	1.0598923797401292e+03
λ_2	2.1924563502992269e+00
λ_3	4.5610942259513210e-01
λ_4	9.4349201788190840e-04

Table 7: Eigenvalues related to the fixed point of the stroboscopic map.

There is a weak unstable direction and also a strong one. The weak direction is related to the $1D$ manifold that appears in a model with one degree of freedom and that it is responsible for the recollisions there [KCUM14]. The strongly unstable direction is consequence of adding the direction which is transversal to the polarization laser. Henceforth, the dynamics near the fixed point of the stroboscoìc map is governed by the strongly unstable direction. The influence of the strong unstable eigendirection makes most of the orbits close to the fixed point get expelled away from the core and do not return back in a few laser cycles. However, it could be possible to find thin strips close to the weak invariant subspace with a lot of recolliding trajectories. Still, it is numerically challenging to compute these $2D$ unstable and stable manifolds and, specially, to globalize the weak $1D$ manifold.

Let Λ_1 and Λ_2 be intervals containing the origin, let $W\colon \Lambda_1 \times \Lambda_2 \to \mathbb{R}^4$ be a parametrization of the $2D$ unstable invariant manifold related to the fixed point, and let P be the stroboscopic map associated to (20). The parametrization of the unstable manifold W must verify the following invariance equation,

$$P(W(s_1, s_2)) = W(\lambda_1 s_1, \lambda_2 s_2).$$

Computing this $2D$ manifold (using double precision) using the parametrization method up to order 8 takes 0.5s. Using MPFR with a mantissa of 128 bits (39 decimal digits) it takes 1 minutes and 19 seconds. Computing up to order 16 requires 15 minutes and 26 seconds. To compute it up to order 30 using a mantissa of 192 bits (around 57 decimal digits) takes 8 hours and 50 minutes. Similarly to the 1D case, we use these different approximations to estimate the error on the coefficients of the expansion. Figure 6 plots the manifold. The computation stops at order 17, when the gain in $\min(s_1^{\max}, s_2^{\max})$ is less than 1.1.

Let us now discuss the globalization of the $1D$ weak unstable manifold (the one related to the

eigenvalue $\lambda \approx 2.1924563502992269$). To start the discussion, assume that we have an approximation to the weak unstable manifold and that p_0 is a point provided by this approximation so we assume it is very close to the true manifold, that is, $p_0+\delta$ is exactly on the manifold and $\|\delta\|$ is very small. When the map P is applied to the point p_0, the error δ is multiplied, approximately, by $\lambda_1 \approx 1059$ at each iteration so that the distance to the weak manifold grows extremely fast. Therefore, it is very convenient to combine a high degree expansion of the manifold (to start the globalization as far as possible from the hyperbolic point) with extended precision. In this situation, it is convenient to accumulate the product of the norms to have an estimate of the growth of the error along the process.

In Table 8, we display an example of the error propagation when globalizing the weak unstable manifold. We select a point on a power expansion of that manifold (computed up to degree 30 with an arithmetic of 60 decimal digits) for the value of the parameter $s = 1$. The first row shows an error estimate of that point (obtained as the size of the contribution of the terms order 30 to the manifold) and the distance to the fixed point. Next rows refer to the iterations of this initial point by the Poincaré map. The second column shows accumulated product of the norms of the differential of the stroboscopic map at each point with the initial error, and the third one the distance to the fixed point. It is clear that, at the beginning, we have a factor growth around 10^3 due to the most unstable eigenvalue. From the table it can be read that, the instability caused by the strongly unstable manifold decreases as the electron move away from the fixed point. This simplifies the approximation of the manifold up to long distances.

iter	error	distance
0	7.996832e-46	1.001406e+00
1	8.466197e-43	2.199796e+00
2	8.928646e-40	4.848533e+00
3	9.240140e-37	1.081419e+01
4	8.411957e-34	2.553592e+01
5	2.083436e-32	1.745048e+01
6	1.966030e-29	1.976583e+01
7	1.310301e-27	7.533221e+01
8	1.615796e-27	1.267686e+02
9	1.771004e-27	1.773365e+02
10	1.873796e-27	2.275002e+02

Table 8: Estimated error for the first 10 iterations for a point in the weak unstable manifold. The third column displays the distance to the fixed point.

This experiment also shows that the propagation of error tends, in some cases, to soften at some distance of the periodic orbit. This example shows the feasibility of the computation of 2D stable/unstable invariant manifolds and their globalization, despite of having very different eigenvalues. The method is based on using a high-order approximation of a parametrization of the 2D unstable manifold combined with extended precision arithmetic.

Acknowledgments

The project leading to this application has received funding from the European Union's Horizon 2020 research and innovation programme under the Marie Skłodowska-Curie grant agreement

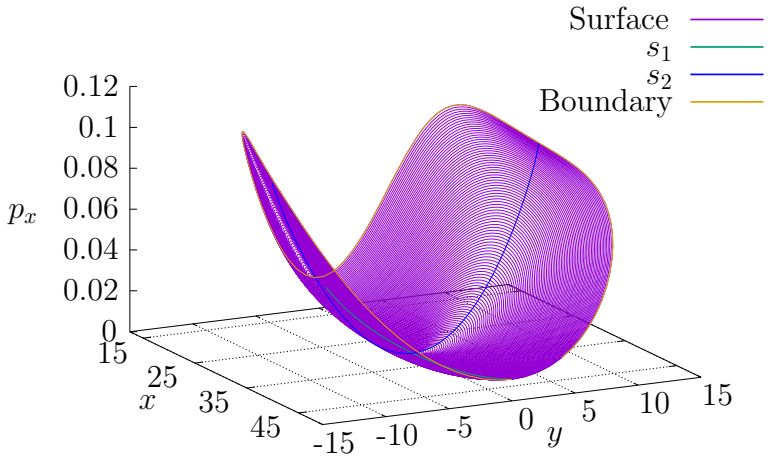

Figure 6: The 2D manifold from the expansion obtained in the parametrization method.

No 734557, the Spanish grant PID2021-125535NB-I00 (MICINN/AEI/FEDER, UE), and the Catalan grant 2017 SGR 1374. J.G. has also been supported with funds from NextGenerationEU within the Spanish national Recovery, Transformation and Resilience plan. N.M. has also been supported by the Spanish grant PID2019-104851GB-I00. M.J.C. has also been supported by Spanish Ministry of Economy and Competitiveness, through the María de Maeztu Programme for Units of Excellence in R&D (CEX2020-001084-M).

References

[ADLBZB10] R. Armellin, P. Di Lizia, F. Bernelli-Zazzera, and M. Berz. Asteroid close encounters characterization using differential algebra: the case of Apophis. *Celest. Mech. Dyn. Astron.*, 107(4):451–470, 2010.

[AFJ+08] E.M. Alessi, A. Farrés, À. Jorba, C. Simó, and A. Vieiro. Efficient usage of self validated integrators for space applications. Ariadna final report, contract no. 20783/07/NL/CB, ESTEC (European Space Agency), 2008.

[AFJ+09] E.M. Alessi, A. Farrés, À. Jorba, C. Simó, and A. Vieiro. Jet transport and applications to neos. In *Proceedings of the 1st IAA Planetary Defense Conference: Protecting Earth from Asteroids*, Granada (Spain), 2009.

[But87] J.C. Butcher. *The Numerical Analysis of Ordinary Differential Equations*. Wiley, 1987.

[CAP] CAPD DynSys Library. `http://capd.ii.uj.edu.pl`.

[CCd13] R. Calleja, A. Celletti, and R. de la Llave. A KAM theory for conformally symplectic systems: efficient algorithms and their validation. *J. Differential Equations*, 255(5):978–1049, 2013.

[CCGd22] R. Calleja, A. Celletti, J. Gimeno, and R. de la Llave. KAM quasi-periodic tori for the dissipative spin–orbit problem. *Commun. Nonlinear Sci. Numer. Simul.*, 106:106099, 2022.

[CFdlL05] X. Cabré, E. Fontich, and R. de la Llave. The parameterization method for invariant manifolds. III. Overview and applications. *J. Differential Equations*, 218(2):444–515, 2005.

[CJ00] E. Castellà and À. Jorba. On the vertical families of two-dimensional tori near the triangular points of the Bicircular problem. *Celest. Mech. Dyn. Astron.*, 76(1):35–54, 2000.

[Cor93] P. B. Corkum. Plasma perspective on strong field multiphoton ionization. *Phys. Rev. Lett.*, 71:1994–1997, Sep 1993.

[Cor14] P. Corkum. Recollision physics. *Physics Today*, 64:36–41, 03 2014.

[CRR64] J. Cronin, P.B. Richards, and L.H. Russell. Some periodic solutions of a four-body problem. *Icarus*, 3:423–428, 1964.

[DJ22] G. Duarte and À. Jorba. Using normal forms to study Oterma's transition in the planar RTBP. *Discrete Contin. Dyn. Syst. Ser. B*, 2022. To appear.

[DJCJC22] J. Dubois, M. Jorba-Cuscó, À. Jorba, and C. Chandre. Dynamical organization of recollisions by a family of invariant tori. *SIAM J. Appl. Dyn. Syst.*, 21(1):523–541, 2022.

[DS92] A. Delshams and T.M. Seara. An asymptotic expression for the splitting of separatrices of the rapidly forced pendulum. *Comm. Math. Phys.*, 150:433–463, 1992.

[FdlL92] C. Falcolini and R. de la Llave. Numerical calculation of domains of analyticity for perturbation theories in the presence of small divisors. *J. Statist. Phys.*, 67(3-4):645–666, 1992.

[Feh68] E. Fehlberg. *Classical Fifth-, Sixth-, Seventh-, and Eighth-order Runge-Kutta Formulas with Stepsize Control.* NASA technical report. National Aeronautics and Space Administration, 1968.

[FHL+07] L. Fousse, G. Hanrot, V. Lefèvre, P. Pélissier, and P. Zimmermann. MPFR: A multiple-precision binary floating-point library with correct rounding. *ACM Trans. Math. Softw.*, 33(2), 2007.

[FR81] V. Franceschini and L. Russo. Stable and unstable manifolds of the Hénon mapping. *J. Statist. Phys.*, 25(4):757–769, 1981.

[GC91] A. Griewank and G.F. Corliss, editors. *Automatic Differentiation of Algorithms: Theory, Implementation, and Application.* SIAM, Philadelphia, Penn., 1991.

[GJJC+] J. Gimeno, À. Jorba, M. Jorba-Cuscó, N. Miguel, and M. Zou. Using jet transport to produce normal forms of Poincaré maps. Work in progress.

[GJNO22] J. Gimeno, À. Jorba, B. Nicolás, and E. Olmedo. Numerical computation of high-order expansions of invariant manifolds of high-dimensional tori. *SIAM J. Appl. Dyn. Syst.*, 21(3):1832–1861, 2022.

[GJZ22] J. Gimeno, À. Jorba, and M. Zou. Taylor package, version 2, 2022. `http://www.maia.ub.es/~angel/taylor`.

[Gri00] A. Griewank. *Evaluating Derivatives*. SIAM, Philadelphia, Penn., 2000.

[HCL+16] A. Haro, M. Canadell, A. Luque, J.-M. Mondelo, and J.-Ll. Figueras. *The Parameterization Method for Invariant Manifolds. From Rigorous Results to Effective Computations*, volume 195 of *Applied Mathematical Sciences*. Springer-Verlag, 2016.

[HNW00] E. Hairer, S. P. Nørsett, and G. Wanner. *Solving ordinary differential equations I. Nonstiff problems*, volume 8 of *Springer Series in Computational Mathematics*. Springer-Verlag, Berlin, second revised edition, 2000.

[Hua60] S.S. Huang. Very restricted four-body problem. Technical note TN D-501, Goddard Space Flight Center, NASA, 1960.

[JCFJ18] M. Jorba-Cuscó, A. Farrés, and À. Jorba. Two periodic models for the Earth-Moon system. *Front. Appl. Math. Stat.*, 4, 2018.

[JPN10] À. Jorba and E.-M. Pérez-Nueno. Propagation of the uncertainty region for a particle around the Earth. Final report, Deimos Space SL, 2010.

[JZ05] À. Jorba and M. Zou. A software package for the numerical integration of ODEs by means of high-order Taylor methods. *Exp. Math.*, 14(1):99–117, 2005.

[KCUM14] A. Kamor, C. Chandre, T. Uzer, and F. Mauger. Recollision scenario without tunneling: Role of the ionic core potential. *Phys. Rev. Lett.*, 112:133003, 04 2014.

[KMCU14] A. Kamor, F. Mauger, C. Chandre, and T. Uzer. How key periodic orbits drive recollisions in a circularly polarized laser field. *Phys. Rev. Lett.*, 25:253002, 07 2014.

[Knu98] D.E. Knuth. *The Art of Computer Programming, Volume 2: Seminumerical Algorithms*. Addison-Wesley, Boston, third edition, 1998.

[KOD+05] B. Krauskopf, H. M. Osinga, E. J. Doedel, M. E. Henderson, J. Guckenheimer, A. Vladimirsky, M. Dellnitz, and O. Junge. A survey of methods for computing (un)stable manifolds of vector fields. *Internat. J. Bifur. Chaos Appl. Sci. Engrg.*, 15(3):763–791, 2005.

[KS17] T. Kapela and C. Simó. Rigorous KAM results around arbitrary periodic orbits for Hamiltonian systems. *Nonlinearity*, 30(3):965–986, 2017.

[Kuz04] Y.A. Kuznetsov. *Elements of applied bifurcation theory*, volume 112 of *Applied Mathematical Sciences*. Springer-Verlag, New York, third edition, 2004.

[LABZB14] P. Di Lizia, R. Armellin, F. Bernelli-Zazzera, and M. Berz. High order optimal control of space trajectories with uncertain boundary conditions. *Acta Astron.*, 93:217 – 229, 2014.

[LAL08] P. Di Lizia, R. Armellin, and M. Lavagna. Application of high order expansions of two-point boundary value problems to astrodynamics. *Celest. Mech. Dyn. Astron.*, 102(4):355–375, 2008.

[MADLBZ15] A. Morselli, R. Armellin, P. Di Lizia, and F. Bernelli Zazzera. A high order method for orbital conjunctions analysis: Monte carlo collision probability computation. *Adv. Space Res.*, 55(1):311 – 333, 2015.

[MCU10] F. Mauger, C. Chandre, and T. Uzer. Recollisions and correlated double ionization with circularly polarized light. *Phys. Rev. Lett.*, 105:083002, Aug 2010.

[MKCU12] F. Mauger, A. Kamor, C. Chandre, and T. Uzer. Delayed double ionization as a signature of hamiltonian chaos. *Phys. Rev. E*, 85:066205, 06 2012.

[MS09] R. Martínez and C. Simó. Non-integrability of Hamiltonian systems through high order variational equations: Summary of results and examples. *Regul. Chaotic Dyn.*, 14(3):323–348, Jun 2009.

[Nau12] U. Naumann. *The art of differentiating computer programs*, volume 24 of *Software, Environments, and Tools*. Society for Industrial and Applied Mathematics (SIAM), Philadelphia, PA, 2012.

[NCUW15] M. J. Norman, C. Chandre, T. Uzer, and P. Wang. Nonlinear dynamics of ionization stabilization of atoms in intense laser fields. *Phys. Rev. A*, 91:023406, Feb 2015.

[PPGM18] D. Pérez-Palau, G. Gómez, and J.J. Masdemont. A new subdivision algorithm for the flow propagation using polynomial algebras. *Commun. Nonlinear Sci. Numer. Simul.*, 61:37–53, 2018.

[PPMG13] D. Pérez-Palau, J. Masdemont, and G. Gómez. Jet Transport propagation of uncertainties for orbits around the Earth. In *Proceedings of the 64th International Astronautical Congress (IAC)*, volume 7, pages 5482–5489, 2013.

[PPMG14] D. Pérez-Palau, J. Masdemont, and G. Gómez. The Jet Transport applied to the detection of Lagrangian Coherent Structures. In *Proceedings of the 2014 ICNPAA: Mathematical Problems in Engineering, Aerospace and Sciences*, 07 2014.

[PPMG15] D. Pérez-Palau, J. Masdemont, and G. Gómez. Tools to detect structures in dynamical systems using jet transport. *Celest. Mech. Dyn. Astron.*, 123(3):239–262, Nov 2015.

[Ric80] D.L. Richardson. A note on a Lagrangian formulation for motion about the collinear points. *Celestial Mech.*, 22(3):231–236, 1980.

[SGJM95] C. Simó, G. Gómez, À. Jorba, and J. Masdemont. The Bicircular model near the triangular libration points of the RTBP. In A.E. Roy and B.A. Steves, editors, *From Newton to Chaos*, pages 343–370, New York, 1995. Plenum Press.

[Sim90] C. Simó. On the analytical and numerical approximation of invariant manifolds. In D. Benest and C. Froeschlé, editors, *Modern methods in celestial mechanics*, pages 285–330. Ed. Frontières, 1990. Reprinted at `http://www.maia.ub.es/dsg/2004/index.html`.

[Sze67] V. Szebehely. *Theory of Orbits*. Academic Press, 1967.

[VADLL13] M. Valli, R. Armellin, P. Di Lizia, and M. R. Lavagna. Nonlinear mapping of uncertainties in celestial mechanics. *J. Guid. Control. Dyn.*, 36(1):48–63, 2013.

[VADLL14] M. Valli, R. Armellin, P. Di Lizia, and M. Lavagna. Nonlinear filtering methods for spacecraft navigation based on differential algebra. *Acta Astron.*, 94(1):363 – 374, 2014.

[WDLA+15] A. Wittig, P. Di Lizia, R. Armellin, K. Makino, F. Bernelli-Zazzera, and M. Berz. Propagation of large uncertainty sets in orbital dynamics by automatic domain splitting. *Celest. Mech. Dyn. Astron.*, 122(3):239–261, 2015.